An interatomic potential for W-N interactions

Polvi, J.

2016-08

Polvi , J , Heinola , K & Nordlund , K 2016 , ' An interatomic potential for W-N interactions ' , Modelling and Simulation in Materials Science and Engineering , vol. 24 , no. 6 , 065007 . https://doi.org/10.1088/096

http://hdl.handle.net/10138/308769
https://doi.org/10.1088/0965-0393/24/6/065007

Preprint of paper: Modelling and Simulation in Materials Science and Engineering. 24, 6, 11 p., 065007.

An interatomic potential for W-N interactions

J. Polvi[a], K. Heinola[a] and K. Nordlund[a,b]

[a] Department of Physics, P.O. Box 43, FI-00014 University of Helsinki, Finland
[b] National Research Nuclear University MEPhI, 115409 Moscow, Russia

E-mail: jussi.polvi@helsinki.fi

Abstract. N_2 gas is s routinely used as seeding species in fusion plasmas to control the amount of power emitted from plasma by radiation to the tungsten walls of ITER-like divertor. Nitrogen atoms will interact with the plasma-facing materials beryllium and tungsten, and form chemical bonds with the wall surfaces, as well as with plasma hydrogen isotopes, thus raising a special interest in W-N and N-H interactions in the fusion community. In this work we describe the development of an analytical interatomic potential for W-N interactions and benchmark the potential against DFT calculation results for N defects in tungsten.

Submitted to: *Modelling and Simulation in Materials Science and Engineering*

1. Introduction

Scientists around the world have been researching controlled fusion, aiming to utilize fusion power for the production of electricity, since the mid-1950s. It has been accompanied with extreme scientific and technological difficulties, but has still resulted in clear progress, though electricity production remains to be demonstrated. In theory, fusion sounds like an ideal energy source; fusing the hydrogen isotopes deuterium (D) and tritium (T) requires only small amounts of fuel, and releases vast amounts of energy with helium as the only by-product [1], in addition to the neutron flow. In practise, unfortunately, controlled fusion has turned out to be a rather elusive target.

The main challenge of terrestrial thermonuclear fusion arises from the temperature requirements; in order to create a deuterium-tritium plasma, the fusion fuel has to be heated up to temperatures about ten times higher than the Sun's core. In *tokamak* reactors this plasma is confined and controlled by strong magnetic field in a toroidal chamber. Since magnetic fields do not hold neutral particles, such as neutralized plasma fuel particles and neutrons, the walls of an active reactor chamber are subject to continuous bombardment. Additionally, fragments of the plasma will unavoidably escape the confinement and come in contact with the reactor walls, a phenomenon called plasma-wall interactions (PWI) [2]. These interactions are among the biggest road blocks on our way to sustainable fusion reactor operation, causing erosion of wall materials, contamination of the plasma by the eroded species, and degradation of the reactor materials.

Currently the biggest experimental effort in the field of fusion research is the International Thermonuclear Experimental Reactor (ITER). ITER is an experimental fusion test reactor aiming to show that commercial energy can be produced from fusion [3]. The ITER plasma-facing reactor materials have been chosen based on numerous criteria and will contain beryllium (first wall) and tungsten (exhaust region, the divertor). As a consequence of the PWI, formation of mixed materials —alloys of unknown composition and properties — is inevitable. This mixing can cause surprising material changes in the worst case leading to sudden operational failures.

Tungsten monocarbide (WC) and mononitride (WN) are getting more attention from physicists and material scientists due to their unique physical and chemical properties such as extreme hardness and chemical inertness [4]. Specifically, WN combines a high hardness with good electrical conductivity, and is considered as a promising meterial for manufacturing of ohmic contacts for microelectronics [5, 4]. There is a particular interest towards WN in the fusion community due to the plans to use N_2 or noble gases as seeding species to reduce the power loads on the tungsten divertor target in ITER. The seeding species will interact with the plasma-facing materials beryllium and tungsten, and, in the case of nitrogen, also form chemical bonds with the wall surfaces as well as with plasma hydrogen isotopes.

There exist few studies of nitrogen interacting with tungsten and plasma [6, 7, 8, 9], and it has been found that only very small fractions of N are accumulated on the W surface and that N is bound in a nitride state [6]. According to experiments [10], WN appears to exist in multitude of phases, and depending on the ambient temperature and the pressure of N_2

gas, the maximum atomic concentration of N in W is between 33 and 66 per cent [11] as shown in Fig. 1. A phase diagram calculated with thermodynamical analysis [12] predicted a NaCl-type structure for tungsten subnitrites and a WC-type hexagonal phase for W_xN_{1-x}, where $x \leq 0.5$. It has also been observed that the accumulation of N on the surface decreases the physical sputtering of W due to the lower W concentration at the surface [6]. However, many basic questions, such as, the energy and temperature dependent retention of nitrogen implanted in tungsten, and the erosion of formed tungsten nitride by deuterium, are still open. This creates a need to better understand W-N and N-H interactions in the fusion relevant conditions.

Gaining this understanding requires studying the materials in such harsh environments, that experiments become difficult or impossible. Thus the need for using computer simulation techniques. One such technique is molecular dynamics simulations, which have proven very helpful in understanding different PWI processes, e.g. by identifying the swift chemical sputtering mechanism in the low energy bombardment of carbon and beryllium [13, 14, 15]. However, in order to be useful, the simulations require accurate potentials for every atomic interaction in the system of interest.

Since interatomic potentials for W-Be [16] and W-C-H [17] interactions have already been developed, the W-N potential is a new important piece of a potential puzzle, soon hopefully containing all most important interactions between the fusion reactor materials.

In this work we describe briefly the potential development process, present the parameters for new bond-order potential for W-N interactions, and test the potential for some defect properties in bulk tungsten.

2. Method

2.1. Potential formalism

The idea behind the bond order potential formalism used in this work was originally proposed by L. Pauling [18] already in 1960. Later the bond-order scheme has been shown [19] to resemble both the tight-binding [20] and the embedded-atom method [21, 22]. Previous studies (e.g. [19, 23, 17]) provide comprehensive descriptions of the analytical bond-order potential (ABOP) method, so a brief overview should suffice here.

In the ABOP method, the total energy E of the system is expressed as a sum over individual bond energies:

$$E = \sum_{i>j} f_{ij}^c(r_{ij}) \Big[V_{ij}^R(r_{ij}) - \underbrace{\frac{b_{ij} + b_{ji}}{2}}_{\overline{b_{ij}}} V_{ij}^A(r_{ij}) \Big]. \tag{1}$$

Here V_{ij}^R and V_{ij}^A are the repulsive and attractive terms, respectively. The functional form of these is a Morse-like pair potential,

$$\begin{aligned} V^R(r) &= \frac{D_0}{S-1} \exp\left(-\beta\sqrt{2S}(r-r_0)\right), \\ V^A(r) &= \frac{SD_0}{S-1} \exp\left(-\beta\sqrt{2/S}(r-r_0)\right), \end{aligned} \tag{2}$$

where D_0 and r_0 are the bond energy and length of the dimer molecule. S is an adjustable parameter here, but it has also a physical meaning [24]; $S < 2$ is typical for semiconductors, $S > 2$ for metals, and $S = 2$ means Eq. 2.1 becomes a normal Morse potential. β is also related to the dimer properties according to

$$\beta = k\frac{2\pi c}{\sqrt{2D_0/\mu}}, \tag{3}$$

where k is the vibration wave number and μ the reduced mass of the dimer.

The cut-off function f_{ij}^c has a following form designed to restrict the interaction range:

$$f^c(r) = \begin{cases} 1, & r \leq R - D, \\ \frac{1}{2} - \frac{1}{2}\sin\left(\frac{\pi}{2}(r-R)/D\right), & |R - r| \leq D, \\ 0, & r \geq R + D. \end{cases} \tag{4}$$

Here, R and D are parameters determining the cutoff range and interval where potential value is smoothly reduced to zero. b_{ij} in (eq. 1) is the bond order term, which includes the three-body interactions and angular dependence,

$$b_{ij} = (1 + \chi_{ij})^{-\frac{1}{2}}, \tag{5}$$

where,

$$\chi_{ij} = \sum_{k(\neq i,j)} f_{ik}^c(r_{ik}) g_{ik}(\theta_{ijk}) e^{2\mu_{ijk}(r_{ij} - r_{ik})}. \tag{6}$$

Here μ_{ik} is a fitting parameter and the angular function g_{ik} has the form

$$g(\theta) = \gamma\left(1 + \frac{c^2}{d^2} - \frac{c^2}{d^2 + (h + \cos\theta)^2}\right), \tag{7}$$

where γ, c, d and h are again adjustable parameters.

In order to make the potential suitable for high energy simulations also, a repulsive term was added to the total energy (Eq. 1) as explained in the Appendix.

2.2. DFT calculations

2.2.1. Building the fitting database for bulk properties In our fitting process the new ABOP potential was fitted to density functional theory (DFT) calculations of various existing and hypothetical tungsten nitride (WN) bulk phases: caesium chloride (CsCl), rock salt (NaCl), zinc blende (ZnS), tungsten carbide (WC) and nickel arsinide (NiAs). (NaCl and WC phased have been observed experimentally. [10]) The results of these calculations can be seen in Table 2.

DFT calculations were done using the Vienna Ab initio Simulation Package (VASP) [25, 26, 27, 28, 29]. In these calculations the projector augmented wave (PAW) method [30] was used as a plane-wave basis, and for pseudopotentials the local density approximation (LDA) potentials [31, 32] were used, both provided in the VASP.

The sampling of k points in the Brillouin zone was done with the Monkhorst-Pack scheme [33] with a mesh of $15 \times 15 \times 15$. The integration over the Brillouin zone was carried out with the Methfessel-Paxton method [34] when relaxing structures, and the linear

tetrahedron method of Blöchl *et al.* [35] to obtain accurate energies of relaxed structures. The energy cutoff value 400 eV was used for all bulk structures and as well as an accuracy threshold of 0.1 meV per atom for energy convergence. For completeness we tested our results also by using the Perdew-Burke-Ernzerhof (PBE) functionals [36], these results closely matched with the LDA results shown in Table 2 with the exception of cohesive energies which were 10-20 per cent lower for all structures.

2.2.2. Modeling N defects in W The DFT calculations for W-N defect systems were also performed with VASP. In this case the electron exchange-correlation was described with the generalized gradient approximation (GGA) and by using the Perdew-Burke-Ernzerhof (PBE) functionals.

The W-N simulation cell comprised of 128 lattice sites in bcc structure, and the k-point mesh was 3x3x3. The W and N electronic properties were calculated by keeping 6 and 5 outermost electrons in the valence, respectively. The energy cut-off was 450 eV, and the electronic structure relaxation convergence criterion was 0.1 meV. For the volumetric and ionic relaxation the conjugate gradient algorithm was used, and the relaxation was stopped after a convergence criterion of 1 meV/Å was reached. The migration barrier for N in W was calculated using the nudged elastic band (NEB) method [37]. The calculation parameters and convergence criteria were kept the same as in the ground state calculations.

3. Results and discussion

When performing the DFT calculations to generate the fitting database of different crystal structures for WN, the NiAs type crystal structure (shown in Fig. 2) was found to be the most stable phase, i.e. the ground state structure. The energy difference between WC and NiAs phase (-16.99 eV and -17.21 eV per formula unit, respectively) may seem rather small, but it was consistent between LDA and PBE methods (0.22 eV vs. 0.20 eV), as were all other relative differences between modelled phases. There are currently no experimental observations [10, 12] of this but the result is in accordance with previous DFT studies by Benhai et al. [38] and Suetin et al. [39]. A recent DFT work by Mehl et al. [9] tested a large number of different vacancy deficit structures for WN with three different DFT functional, and even though their results varied depending on the functional used, they seemed indicate that some of those more exotic structures might be more stable than the more regular crystal structures tested here. Testing how these structures could be modelled with our potential will be left as a future study for now.

The potential parameters shown in Table 1 were found by searching for parameters that reproduce the properties of structures included in the fitting database as close as possible, with special interest in the properties of the ground state. In this fitting process we utilized fitting code Pontifix [40] developed by Paul Erhart. When a satisfactory set was found, the potential was tested against some properties not included in the first automatized step and if not performing adequately, a new parameter set was investigated. More details about the fitting process can be found from [17, 16].

The agreement of the W-N potential with the fitting data is seen in Table 2. The lack of experimental data to compare with makes a comprehensive evaluation difficult. However, the structural properties for most of the structures in fitting data base were reproduced well with the ABOP, and for the ground state structure, the bulk modulus B and pressure derivative B' were also in excellent agreement with the DFT results. Unfortunately for the elastic constants, the parameter set produced rather poor agreement. After numerous iterations through different parameter sets it appears that this is an unavoidable compromise.

One possible issue worth noting with this new potential parameter set is that, unlike the Be-W potential by Björkas et al. [16] and W-C-H potential by Juslin et al. [17], this potential uses new W-W parameters by Ahlgren et al. [41]. Even though this choice makes it more difficult to use the new ABOP together with these older potentials, this was deemed necessary as the older W-W parameter have been shown to give too low defect formation energies and wrong self-interstitial atom configuration for W [41].

The most interesting feature of a new potential is not its ability to describe features which it is fitted to describe, but how it performs in describing features outside it's fitting database. For this purpose we performed series of DFT calculations on interstitial and substitutional N in bulk W and then compared the results with the new ABOP.

In Table 3 we have compared the DFT and MD results for a monovacancy, N defects and some combinations of these in bulk W. The calculation of energy of a vacancy in W doesn't include N, so it doesn't use the new ABOP. The energy of the interstitial N is in very good agreement with DFT, whereas the binding energy between two interstitial N is underestimated with the new potential, because the interstitial distance (3.2 Å) is longer than the cut-off for N-N interactions (2.5 Å). However, since this cut-off value comes from the previously developed N-N potential [42] and increasing caused compatibility issues, we decided to keep it unchanged. The binding energy between a N atom and a monovacancy in W is 2.571 eV in DFT and 1.795 eV in ABOP, and for a second N atom added to the monovacancy, 2.431 eV and 1.729 eV, respectively. Both values are in reasonable agreement and remarkably reproduce the trend from DFT, as N1 and N2 have nearly equal binding energies with the monovacancy. By contrast, the binding energy for a third N is close to zero in DFT and clearly positive in the new ABOP. Even though this is poor agreement in a mathematical sense, for the physical properties the results agree; the binding energy is so small in DFT that the 3rd N is not stable at room temperature and only two N fit in monovacancy in tungsten.

We also tested the performance of the ABOP by performing NEB calculations of moving one interstitial N from one stable position to another in bulk W. The path and results are visualized in Fig. 3. The energy barrier was 0.78 eV in DFT and 0.624 eV with the new potential, both the shape and height of the barrier being in good agreement between the two methods.

4. Conclusions

The new ABOP presented here is fitted to properties of set of different W-N bulk structures, matching well with the structural properties predicted by DFT calculations. When applying the potential to a topic outside its fitting database, our preliminary tests showed the new ABOP reproduced the DFT results of N defects in W with mostly excellent accuracy. This potential could be used to model the effects of N_2 seeding for ITER-like tungsten divertor. Next step will be to create potential parameters for W-H and N-H interactions also, allowing us to model the chemistry between the N_2 gas and plasma hydrogen isotopes as well as the PWI effects in divertor.

Acknowledgments

This work has been carried out within the framework of the EUROfusion Consortium and has received funding from the Euratom research and training programme 2014–2018 under grant agreement No 633053. The views and opinions expressed herein do not necessarily reflect those of the European Commission. Grants of computer time from the Center for Scientific Computing (CSC) in Espoo, Finland are gratefully acknowledged.

Appendix A. Modification of the repulsive potential

The repulsive part of the potentials was modified in a manner previously used for Tersoff-like many body potentials [19, 43]: A total potential V_{Tot} was constructed by joining the original universal ZBL repulsive potential $V_{ZBL}(r)$ [44] with the equilibrium potential $V_{Eq}(r)$ using

$$V_{Tot}(r) = V_{ZBL}(r)(1 - F(r)) + V_{Eq}(r)F(r), \tag{A.1}$$

where V_{Eq} is the potential for states close to equilibrium described in the main text and the Fermi function

$$F(r) = \frac{1}{1 + e^{-b_f(r-r_f)}}. \tag{A.2}$$

Note that the Fermi function is used here merely as a function which smoothly goes from 1 to 0 in a relatively narrow r interval, with no connection to the Fermi level of the electrons of the solid. The value of the constants b_f and r_f are manually chosen so that the potential is essentially unmodified at the equilibrium and longer bonding distances, and that a smooth fit at short separations with no spurious minima is achieved for all realistic coordination numbers. The parameters for each potential are found in table 1. The same parameters were also found to give a smooth fit to the dimer pair repulsive potential calculated with the DMol code [45].

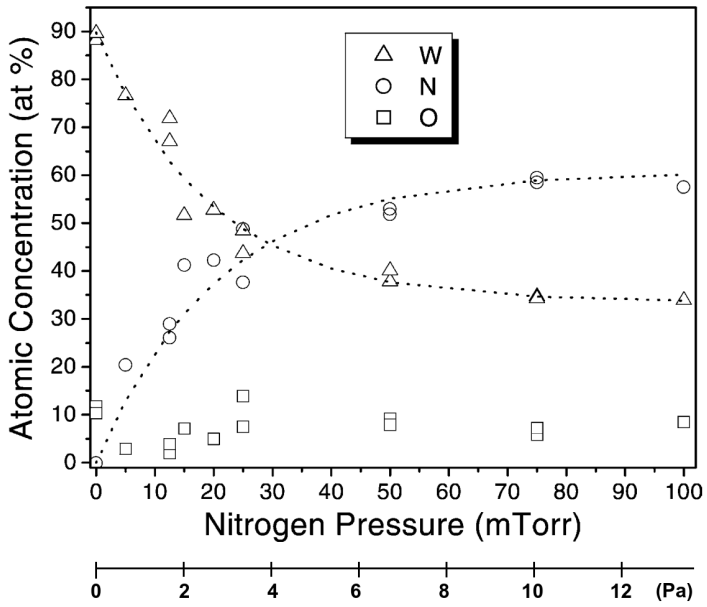

Figure 1. W (triangles), N (circles) and O (squares) relative atomic concentrations determined by high-resolution XPS as a function of nitrogen depositing pressure. Reproduced from [11].

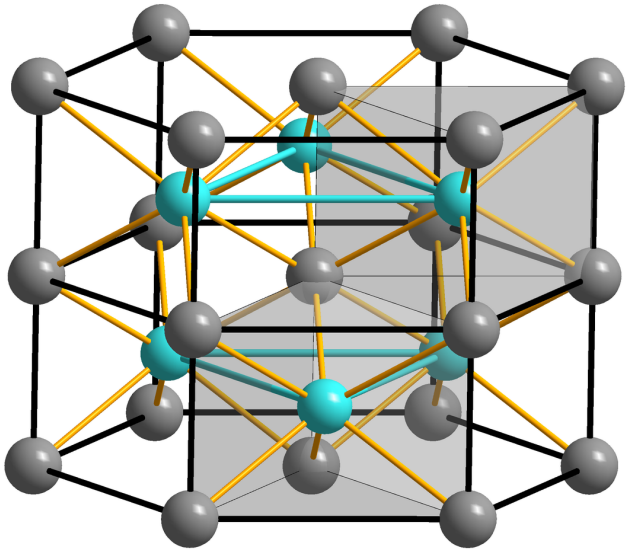

Figure 2. The WN ground state structure: NiAs (W as Ni, N as As). The W6N trigonal prisms are shaded gray and one octahedron of six N atoms surrounding a W atom is shown in the center of the figure. Picture source [46].

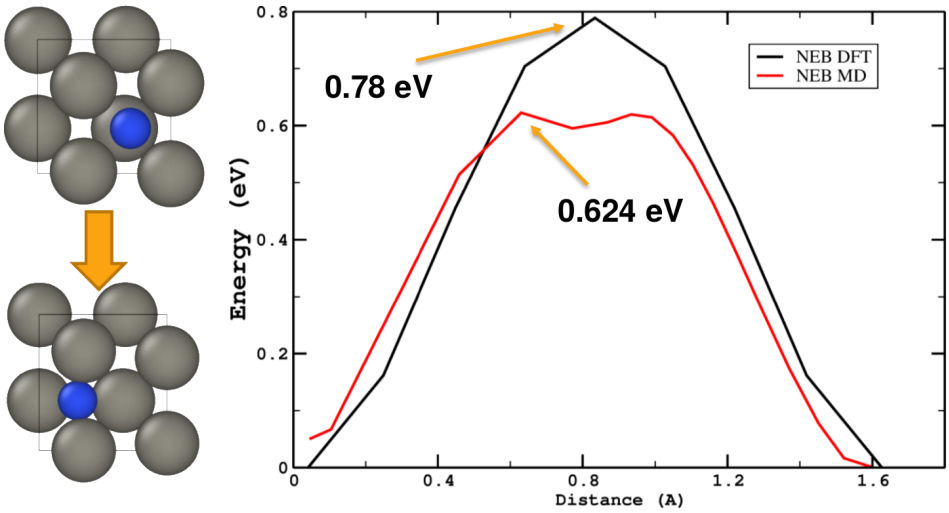

Figure 3. Energy required to move a interstitial N from one stable position to another in bulk W (BCC lattice). The data from NEB calculations is giving a comparison between DFT and the new potential.

Tables and table captions

Table 1. Parameter sets for the different interaction types. The N-N parameters are taken from Ref [42] and the W-W from Ref [41]

	W-W	N-N	W-N
D_0 (eV)	3.282547	9.910000	7.830000
r_0 (Å)	2.460687	1.110000	1.780000
β (Å^{-1})	1.373146	2.059450	1.130000
S	2.215376	1.492200	2.280000
γ	0.001294	0.766120	0.000091
c	1.327324	0.178493	72.000000
d	0.135096	0.201720	0.710885
h	-0.352000	0.045234	1.000000
R (Å)	4.400000	2.300000	2.830000
D (Å)	0.840189	0.200000	0.820000
2μ	0.0	0.0	0.0
b_f (Å^{-1})	12.0	12.0	12.0
r_f (Å)	1.3	0.5	0.4

Table 2. Properties of various tungsten nitrate bulk phases (both hypothetical and existing ones) as obtained from DFT calculations and using the analytical potential derived in this work. The notation is as follows. E_{coh}: cohesive energy; r, r_2: 1st and 2nd nearest neighbor distances; c/a: ratio of lattice parameters (hexagonal structures); V unit volume; B: bulk modulus; and B': pressure derivative of the bulk modulus. Cohesive energy and unit volume are reported per formula unit.

	DFT	ABOP	Diff. (%)
Dimer			
E_{coh} (eV/f.u.)	-7.47	-7.83	+4.82
r (Å)	1.65	1.78	+7.88
Zinc blende (ZnS, B3, F$\overline{4}$3m, no. 216)			
E_{coh} (eV/f.u.)	-16.19	-14.8792	-8.10
r (Å)	1.9919	2.0885	+4.85
r_2 (Å)	3.2528	3.4104	+4.85
V (Å^3/f.u.)	24.3355	28.0485	+15.26
Rock salt (NaCl, B1, Fm$\overline{3}$m, no. 225)			
E_{coh} (eV/f.u.)	-16.17	-15.5019	-4.13
r (Å)	2.15 (2.18[a])	2.2395	+4.16
r_2 (Å)	3.0456	3.1671	+4.16
V (Å^3/f.u.)	19.8767	22.4639	+13.02
Cesium chloride (CsCl, B2, Pm$\overline{3}$m, no. 221)			
E_{coh} (eV/f.u.)	-15.4700	-16.4735	+6.49
r (Å)	2.32	2.3335	+0.58
r_2 (Å)	2.6789	2.6945	+0.58
V (Å^3/f.u.)	19.2253	22.4639	+13.02
Tungsten carbide (WC, Bh, P$\overline{6}$m2, no. 187)			
E_{coh} (eV/f.u.)	-16.99	-17.1522	+0.95
r (Å)	2.1704	2.3335	+7.52
r_2 (Å)	2.8417 (2.893[b])	3.0553	+7.52
c/a	1.0 (0.977[b])	1.0	0.0
V (Å^3/f.u.)	19.8735 (20.48[b])	24.6960	+24.26
Nickel Arsenide (NiAs,P6$_3$/mmc, no. 194)			
E_{coh} (eV/f.u.)	-17.21	-17.367	+0.91
r (Å)	2.1618	2.2312	+3.21
r_2 (Å)	2.8119	2.8901	+2.78
c/a	1.0153	1.0250	+0.95
V (Å^3/f.u.)	19.5499	21.4294	+9.61
B (GPa)	416[c]	401	-3.66
B'	4.525	4.36	-3.65
C_{11} (GPa)	729[c]	236	-67.62
C_{12} (GPa)	232[c]	98	-57.76
C_{13} (GPa)	244[c]	660	+170.49
C_{33} (GPa)	878[c]	298	-66.06
C_{44} (GPa)	320[c]	399	+24.69

[a] Experimental data from Ref. [47]

[b] Experimental data from Ref. [48]

[c] DFT results from Ref. [38]

Table 3. Testing the new potential for N defect properties in bulk W. The notation is as follows. E_{vacancy}: vacancy formation energy in W, E_{Nint}: energy of interstitial N in W, $E_{\mathrm{N-Nint.bond}}$: bonding energy between two interstitial N atoms, and $E_{\mathrm{V1N1-3}}$: binding energies between vacancy and N defects.

	DFT	ABOP
E_{vacancy} (eV)	-3.329	-5.6754[a]
E_{Nint} (eV)	6.856	7.062
$E_{\mathrm{N-N\ int.bond}}$ (eV)	0.288	0.042
E_{V1N1} (eV)	2.571	1.795
E_{V1N2} (eV)	2.431	1.729
E_{V1N3} (eV)	0.034	-1.459

[a] The vacancy is pure W so the new potential is not used, just the W-W potential from [41].

[1] J. Wesson, *Tokamaks*. Number 48 in Oxford Engineering Series. Clarendon Press, Oxford, 2nd edition, 1997.

[2] R. Parker, G. Janeschitz, H.D. Pacher, D. Post, S. Chiocchio, G. Federici, P. Ladd, ITER Joint Central Team, and Home Teams, Plasma-wall interactions in ITER. *Journal fo Nuclear Materials*, 241-243:1–26, 1997.

[3] *The ITER Organization* http://www.iter.org/.

[4] D. V. Suetin, I. R. Shein and A. L. Ivanovskii, Tungsten carbides and nitrides and ternary systems based on them: the electronic structure, chemical bonding and properties. *Russian Chemical Reviews*, 79(7):611–634, 2010.

[5] R. Freer, The Physics and Chemistry of Carbides, Nitrides and Borides NATO ASI Ser. E, Vol. 185, Kluwer Academic, 1990

[6] K. Schmid, A. Manhard, Ch. Linsmeier, A. Wiltner, T. Schwarz-Selinger, W. Jacob and S. Mändl, Interaction of nitrogen plasmas with tungsten. *Nuclear Fusion*, 50(2):025006, 2010.

[7] G. Meisl, K. Schmid, O. Encke, T Höschen, L. Gao and Ch. Linsmeier, Implantation and erosion of nitrogen in tungsten. *New Journal of Physics*, 16(9):093018, 2014.

[8] G. Meisl, Simulating the Nitrogen Migration in Be/W Tokamaks with WallDYN. Proceedings of 15th International Conference on Plasma-Facing Materials and Components for Fusion Applications, 18th May 2015 – 22nd May 2015, Aix-en-Provence, France.

[9] M.J. Mehl, D. Finkenstad, C. Dane, G.L.W. Hart and S. Curtarolo, Finding the stable structures of $N_{1-x}W_x$ with *ab inition* high-throughput approach *Physical Revier B*, 91:184110, 2015.

[10] H.A. Wriedt, The N-W (nitrogen-tungsten) system. *Bulletin of Alloy Phase Diagrams*, 10(4):358–367.

[11] G. Soto, W. de la Cruz, F.F. Castillón, J.A. Díaz, R. Machorro and M.H. Farías. Tungsten nitride films grown via pulsed laser deposition studied in situ by electron spectroscopies. *Applied Surface Science*, 214(1–4):58–67, 2003.

[12] A. Fernández Guillermet, and S. Johnsson, Thermodynamic Analysis of Stable and Metastable W Nitrides and Calculation of W-N phase Diagram *Z. Metallkd.* 84(2):106–117, 1993.

[13] K. Nordlund, E. Salonen, A. V. Krasheninnikov, and J. Keinonen, Swift chemical sputtering of covalently bonded materials. *Pure and Applied Chemistry*, 78(6):1203–1212, 2006.

[14] P. S. Krstic, C. O. Reinhold, and S. Stuart, Chemical sputtering from amorphous carbon under bombardment by deuterium atoms and molecules. *New J. Phys.*, 9:209, 2007.

[15] C. Björkas, K. Vörtler, K. Nordlund, D. Nishijima, and R. Doerner, Chemical sputtering of Be due to D bombardment. *New Journal of Physics*, 11:123017, 2009.

[16] C. Björkas, K. O. E. Henriksson, M. Probst and K. Nordlund, A Be-W interatomic potential. *Journal of Physics: Condensed Matter*, 22:352206, 2010.

[17] N. Juslin, P. Erhart, P. Träskelin, J. Nord, K. O. E. Henriksson, K. Nordlund, E. Salonen, and K. Albe, Analytical interatomic potential for modelling non-equilibrium processes in the w-c-h system. *J. Appl. Phys.*, 98:123520, 2005.

[18] L. Pauling, *The nature of the chemical bond*. Cornell University Press, Ithaca, third edition, 1960.

[19] K. Albe, K. Nordlund, and R. S. Averback, Modeling metal-semiconductor interaction: Analytical bond-order potential for platinum-carbon. *Phys. Rev. B*, 65:195124, 2002.

[20] F. Cleri and V. Rosato, Tight-binding potentials for transition metals and alloys. *Phys. Rev. B*, 48(1):22, 1993.

[21] M. S. Daw and M. I. Baskes, Embedded-atom method: Derivation and application to impurities, surfaces, and other defects in metals. *Physical Review B*, 29:6443–6453, 1984.

[22] D. Brenner, Relationship between the embedded-atom method and tersoff potentials. *Phys. Rev. Lett.*, 63:1022, 1989.

[23] J. Nord, K. Albe, P. Erhart, and K. Nordlund, Modelling of compound semiconductors: Analytical bond-order potential for gallium, nitrogen and gallium nitride. *Journal of Physics: Condensed Matter*, 15(32):5649–5662, 2003.

[24] G. C. Abell, Empirical chemical pseudopotential theory of molecular and metallic bonding. *Physical Review B*, 31(10):6184–6196, 1985.

[25] G. Kresse and J. Hafner, Ab initio molecular dynamics for liquid metals. *Phys. Rev. B*, 47(1):558–561, 1993.

[26] G. Kresse and J. Hafner, Ab initio molecular-dynamics simulation of the liquid-metal-amorphous-semiconductor transition in germanium. *Phys. Rev. B*, 49(20):14251–14269, 1994.

[27] G. Kresse and J. Furthmüller, Efficiency of ab-initio total energy calculations for metals and semiconductors using a plane-wave basis set. *Comp. Mater. Sci.*, 6:15–50, 1996.

[28] G. Kresse and J. Furthmüller, Efficient iterative schemes for ab initio total-energy calculations using a plane-wave basis set. *Phys. Rev. B*, 54(16):11169–11186, 1996.

[29] G. Kresse and D. Joubert, From ultrasoft pseudopotentials to the projector augmented-wave method. *Phys. Rev. B*, 59(3):1758–1775, 1999.

[30] P. E. Blöchl, Projector augmented-wave method. *Phys. Rev. B*, 50(24):17953–17979, 1994.

[31] D. M. Ceperley and B. J. Alder, Ground State of the Electron Gas by a Stochastic Method. *Phys. Rev. Lett.*, 45(7):566–569, 1980.

[32] J. P. Perdew and Alex Zunger, Self-interaction correction to density-functional approximations for many-electron systems. *Phys. Rev. B*, 23(10):5048–5079, 1981.

[33] H. J. Monkhorst and J. D. Pack, Special points for brillouin-zone integrations. *Phys. Rev. B*, 13(12):5188–5192, 1976.

[34] M. Methfessel and A. T. Paxton, High-precision sampling for brillouin-zone integration in metals. *Phys. Rev. B*, 40(6):3616–3621, 1989.

[35] P. E. Blöchl, O. Jepsen, and O. K. Andersen, Improved tetrahedron method for brillouin-zone integrations. *Phys. Rev. B*, 49(23):16223–16233, 1994.

[36] J.P. Perdew, K. Burke and M. Ernzerhof, Matthias, Generalized Gradient Approximation Made Simple *Phys. Rev. Lett.*, 77(18):3865–3868, 1996.

[37] G. Henkelman and H. Jönsson, Improved tangent estimate in the nudged elastic band method for finding minimum energy paths and saddle points. *The Journal of chemical physics*, 113(22):9978–9985, 2000.

[38] Y. Benhai, W. Chunlei, S. Xuanyu, S. Qiuju and C. Dong, Structural stability and mechanical property of WN from first-principles calculations. *Journal of Alloys and Compounds*, 487:556–559, 2009

[39] D. V. Suetin, I. R. Shein and A. L. Ivanovskii, Elastic and electronic properties of hexagonal and cubic polymorphs of tungsten monocarbide WC and mononitride WN from first-principles calculations. *phys. stat. sol. (b)*, 245(8):1590–1597, 2008.

[40] P. Erhart, *Intrinsic Point Defects in Zinc Oxide: Modeling of Structural, Electronic, Thermodynamic and Kinetic Properties* PhD Thesis, Available online at: http://elib.tu-darmstadt.de/diss/000726

[41] T. Ahlgren, K. Heinola, N. Juslin and A. Kuronen, Bond-order potential for point and extended defect simulations in tungsten. *Journal of Applied Physics*, 107(3):033516, 2010.

[42] K. Albe, J. Nord and K. Nordlund, Dynamic charge-transfer bond-order potential for gallium nitride. *Philosophical Magazine*, 89(34-36):3477-3497, 2009.

[43] C. Björkas and K. Nordlund, Comparative study of cascade damage in Fe simulated with recent potentials. *Nuclear Instruments and Methods in Physics Research B*, 259:853–860, 2007.

[44] J. F. Ziegler, J. P. Biersack, and U. Littmark, *The Stopping and Range of Ions in Matter*. Pergamon, New York, 1985.

[45] K. Nordlund, N. Runeberg and D. Sundholm, Repulsive interatomic potentials calculated using Hartree-Fock and density-functional theory methods. *Nucl. Instr. Meth. Phys. Res. B*, 132:45–54, 1997.

[46] Orci (artist) 18 January 2009 - Data from: J.G. Thomson et.al. The crystal structure of nickel arsenide. *J. Phys. C: Solid State Phys*, 21:4007–4013, 1988.

[47] Jeffrey C. Grossman, Ari Mizel, Michel Côté, L. Marvin, and Steven G. Louie, Transition metals and their carbides and nitrides: Trends in electronic and structural properties. *Phys. Rev. B*, 60(9):6343–6347, 1999.

[48] H. J. Goldschmidt, *Interstitial Alloys.* London: Butterworths, 1967